Formation and Characterization of the $(\eta^2\text{-}H_2)CrO_2$, $(\eta^2\text{-}H_2)_2CrO_2$ and HCrO(OH) Molecules

Mingfei Zhou,* Luning Zhang, Limin Shao, Wenning Wang, Kangnian Fan, and Qizong Qin

Department of Chemistry, Laser Chemistry Institute, Fudan University, Shanghai 200433, P. R. China

Received: May 2, 2001; In Final Form: August 23, 2001

Chromium dioxide dihydrogen and bis-dihydrogen complexes: $(\eta^2\text{-}H_2)CrO_2$ and $(\eta^2\text{-}H_2)_2CrO_2$ have been prepared by co-condensation of the CrO_2 molecules generated from laser ablation of CrO_3 with H_2 in excess argon at 11 K. Broad-band photolysis of the $(\eta^2\text{-}H_2)CrO_2$ complex induced a photoisomerization to produce the HCrO(OH) molecule. In addition, laser-ablated Cr atoms reacted with H_2/O_2 mixtures to give primarily the CrO_2 and $(\eta^2\text{-}O_2)CrO_2$ molecules, while the $(\eta^2\text{-}H_2)CrO_2$, $(\eta^2\text{-}H_2)_2CrO_2$ and HCrO(OH) molecules were also produced on annealing and photolysis. The aforementioned species were unambiguously characterized by FTIR spectroscopy and density functional theoretical calculations.

Introduction

Transition metal dihydrogen complexes are of fundamental importance in a wide variety of processes such as hydroformylation and hydrogenation.[1] The synthesis, structure, and bonding of these complexes and their reactivity have been intensively studied.[2−6] Dihydrogen complexes of chromium have also received considerable attentions.[7−12] A number of chromium metal complexes containing $\eta^2\text{-}H_2$ together with various ligands, such as PR_3, Cp, CO, etc., have been generated photochemically and studied spectroscopically in various low-temperature matrixes as well as in hydrocarbon solvent at room temperature.[7−9] Reactions of chromium atoms with dihydrogen have also been studied both experimentally and theoretically.[13−16] In low-temperature matrixes, chromium atoms are photoreactive toward dihydrogen to give chromium hydride molecules.[13,14]

Chromium oxo species have been used for H−H and C−H bond activation in the gas phase.[17,18] Mass spectrometric studies indicated that chromium dioxide cation slowly reacts with H_2 to form CrO^+ and H_2O, while thermalized CrO^+ does not react with H_2.[18,19] However, little is known about the chromium oxide−dihydrogen complexes or hydrides. In this paper, we report a study of combined matrix-isolation FTIR spectroscopic and density functional theoretical study of the first chromium dioxide dihydrogen and bis-dihydrogen complexes $(\eta^2\text{-}H_2)CrO_2$ and $(\eta^2\text{-}H_2)_2CrO_2$. These complexes can be prepared by reactions of laser-ablated CrO_2 molecules with H_2 or chromium atoms with O_2/H_2 mixture in solid argon. The $(\eta^2\text{-}H_2)CrO_2$ complex rearranges to HCrO(OH) on photolysis.

Experimental and Computational Methods

The experiment for laser ablation and matrix isolation spectroscopy has been described in detail previously.[20] The 1064 nm Nd:YAG laser fundamental (Spectra Physics, DCR 2, 20 Hz repetition rate and 8 ns pulse width) was focused onto a rotating target (CrO_3 or Cr) through a hole in a CsI window. Typically, 5−10 mJ/pulse laser power was used. The ablated species were codeposited with reagent gases in excess argon onto the 11 K CsI window at a rate of 5 mmol/h. The CsI window was mounted on a copper holder at the cold end of the cryostat (Air Products Displex DE202) and maintained by a closed-cycle helium refrigerator (Air Products Displex IR02W). A Bruker IFS 113v FTIR spectrometer equipped with a DTGS detector was used to record the IR spectra in the range of 400−4000 cm^{-1} with a resolution of 0.5 cm^{-1}. Matrix samples were annealed at different temperatures, and selected samples were subjected to broad-band photolysis using a 250 W high-pressure mercury lamp. The annealing experiments were done by warming the sample deposit to the desired temperature and quickly cooling to 11 K.

To provide insight into the structure and bonding in $(\eta^2\text{-}H_2)CrO_2$, $(\eta^2\text{-}H_2)_2CrO_2$ and HCrO(OH), we performed density functional theoretical calculations, which can provide very reliable predictions of structures, binding energies, and vibrational frequencies of transition metal compounds.[21−23] DFT calculations were carried out using the Gaussian 98 program.[24] The three-parameter hybrid functional according to Becke with additional correlation corrections due to Lee, Yang, and Parr was utilized (B3LYP).[25,26] The 6-311++G(d,p) basis sets were used for H and O atoms, and the all electron basis set of Wachters−Hay as modified by Gaussian was used for Cr atom.[27,28] The geometries were fully optimized, harmonic vibrational frequencies were calculated with analytic second derivatives, and zero point vibrational energies (ZPVE) were derived. Transition state optimizations were done with the synchronous transit-guided quasi-Newton (STQN) method at the B3LYP/6-311++G(d,p) level.[29] Population analysis was carried out using the NBO method.[30]

Results and Discussion

Infrared Spectra. *CrO_3 + H_2/Ar.* Laser ablation of a CrO_3 target followed by condensation with pure argon at 11 K formed CrO_2 (965.3 and 914.3 cm^{-1}) as the major product with minor CrO (846.8 cm^{-1}), CrOCrO (984.2 cm^{-1}), and CrO_3 (968.4 cm^{-1}).[31,32] Distinct new product absorptions were observed in experiments using H_2/Ar as reagent gas. Figure 1 shows the representative spectra in selected regions with a H_2/Ar (1.0% molar ratio) sample, and the product absorptions are listed in Table 1. On the basis of the annealing and photolysis behavior, the new product absorptions can be classified into three groups (labeled as **1**−**3** in Figure 1). Band set **2** increased on annealing at the expense of band set **1**. Photolysis markedly decreased band sets **1** and **2** with co-current growth of band set **3**.

* Corresponding author. E-mail: mfzhou@fudan.edu.cn. Fax: +86-21-65102777.

10.1021/jp0116611 CCC: $20.00
Published on Web 11/02/2001

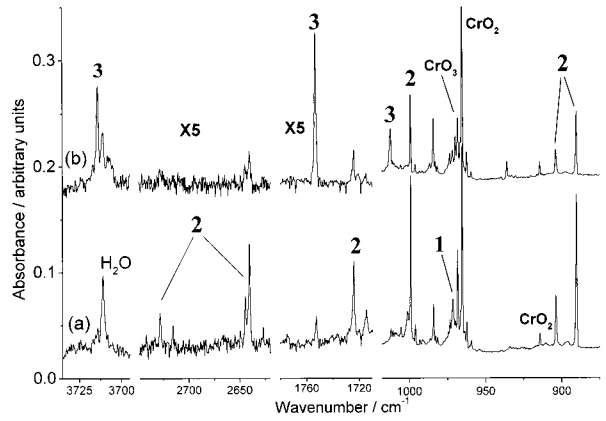

Figure 1. Infrared spectra in selected regions from co-deposition of laser-ablated CrO_3 in 1.0% H_2 in argon: (a) with 1 h sample deposition; (b) after 20 min Hg lamp photolysis.

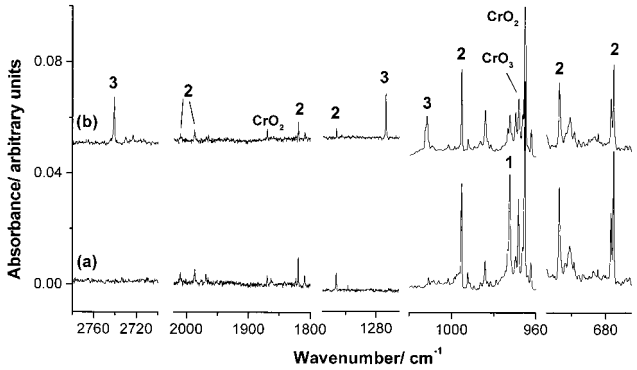

Figure 2. Infrared spectra in selected regions from co-deposition of laser-ablated CrO_3 in 0.8% D_2 in argon: (a) with 1 h sample deposition; (b) after 20 min Hg lamp photolysis.

TABLE 1: Infrared Absorptions (cm^{-1}) from Co-deposition of Laser-Ablated CrO_3 with H_2 or Cr with $H_2 + O_2$ in Excess Argon

H_2	D_2	$^{18}O_2$	$H_2 + D_2$	assignment, mode
3714.2	2740.9	3702.7	3714.2, 2740.9	HCrO(OH) O−H
2728.6	2009.5			$(\eta^2\text{-}H_2)_2CrO_2$ sym H−H
2640.5	1987.1			$(\eta^2\text{-}H_2)_2CrO_2$ asym H−H
1877.7	1819.4			$(\eta^2\text{-}H_2)_2CrO_2$ comb asym + sym OCrO
1869.8	1869.8	1789.8		CrO_2 comb asym + sym OCrO
1753.1	1267.5	1753.1	1753.1, 1267.5	HCrO(OH) Cr−H
1724.1	1332.4			$(\eta^2\text{-}H_2)_2CrO_2$ asym + sym Cr−H_2
1012.3	1011.8	971.6		HCrO(OH) Cr−O
999.2	995.4	963.8	999.2, 997.8, 995.4	$(\eta^2\text{-}H_2)_2CrO_2$ asym $O^{52}CrO$
996.1	992.3	960.6		$(\eta^2\text{-}H_2)_2CrO_2$ asym $O^{53}CrO$
993.2	989.5			$(\eta^2\text{-}H_2)_2CrO_2$ asym $O^{54}CrO$
984.2	984.2			CrOCrO Cr−O
973.8	973.8	936.8		$(\eta^2\text{-}O_2)CrO_2$ asym OCrO
971.7	971.7	935.7		$(CrO_2\text{-}X)$ asym OCrO
971.6	972.5	935.0	972.5, 971.6	$(\eta^2\text{-}H_2)CrO_2$ asym OCrO
968.4	968.4			CrO_3 asym OCrO
965.3	965.3	929.1		$^{52}CrO_2$ asym OCrO
962.4	962.4	926.1		$^{53}CrO_2$ asym OCrO
914.3	914.3	869.6		$^{52}CrO_2$ sym OCrO
906.8	906.8	874.1		$^{52}CrO_2$- asym OCrO
903.8	707.6	876.7	903.8, 897.3, 707.6	$(\eta^2\text{-}H_2)_2CrO_2$ sym H_2CrH_2
890.3	675.6	890.3	890.3, 690.0, 675.6	$(\eta^2\text{-}H_2)_2CrO_2$ asym H_2CrH_2
624.0	457.1	623.5	624.0, 547.8, −	$(\eta^2\text{-}H_2)_2CrO_2$ Cr−H_2 bending

Identical laser ablation investigations were done with D_2/Ar samples, the new product absorptions were shifted as given in Table 1, and the spectra in selected regions are shown in Figure 2. Experiments were also done with mixed $H_2 + D_2$/Ar and $H_2 + HD + D_2$/Ar samples. Figure 3 illustrates the spectra in the 1005−960, 910−885, and 715−665 cm^{-1} regions using different isotopic samples.

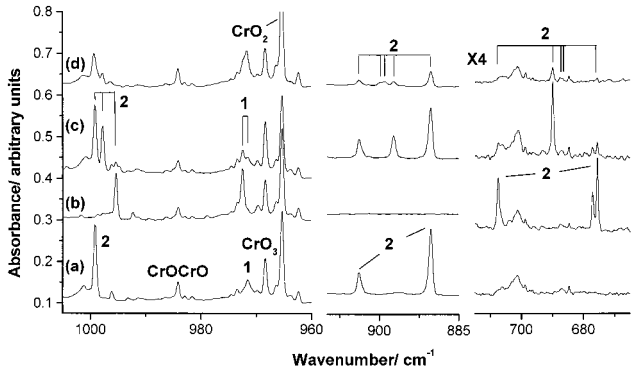

Figure 3. Infrared spectra in the 1005−960, 910−885, and 715−665 cm^{-1} regions from co-deposition of laser-ablated CrO_3 with isotopic H_2 in argon at 11 K: (a) 1.0% H_2; (b) 0.8% D_2; (c) 0.5% H_2 + 0.5% D_2; (d) 0.4% H_2 + 0.8% HD + 0.4% D_2.

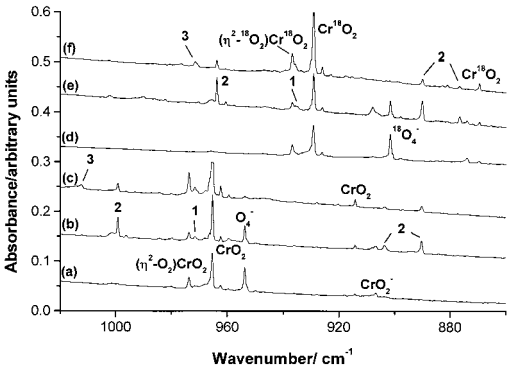

Figure 4. Infrared spectra in the 1020−860 cm^{-1} region from co-deposition of laser-ablated Cr atoms with 1.0% H_2 + 0.5% O_2 in argon: (a) 1.0% H_2 + 0.5% $^{16}O_2$ with 1 h sample deposition, (b) after 18 K annealing, (c) after 20 min photolysis; (d) 1.0% H_2 + 0.5% $^{18}O_2$ with 1 h sample deposition, (e) after 18 K annealing, and (f) after 20 min photolysis.

Cr+O2/H2/Ar. Laser ablation of a Cr metal target and co-deposition in O_2/Ar produced CrO_2, $(\eta^2\text{-}O_2)CrO_2$ (973.8, 918.2 cm^{-1}), CrO_2^- (906.8 cm^{-1}), and O_4^- (953.8 cm^{-1}) absorptions.[31−33] Annealing to 25 and 30 K decreased the $(\eta^2\text{-}O_2)$-CrO_2, CrO_2^-, and O_4^- absorptions and produced weak CrO_3 (968.4 cm^{-1}) absorption. Similar experiments using 1.0% H_2/0.5%O_2/Ar were also done, and the spectra in the 1020−880 cm^{-1} region are shown in Figure 4. Sample deposition at 11 K also produced CrO_2, $(\eta^2\text{-}O_2)CrO_2$, CrO_2^-, and O_4^- absorptions, sample annealing to 18 K produced new absorptions at 971.6 cm^{-1} and band set **2**. Broad-band Hg arc irradiation destroyed species **2** and produced species **3**. Experiments using $H_2/^{18}O_2$/Ar were also done, and the spectra are also shown in Figure 4. All absorptions in the Cr−O stretching vibrational frequency region exhibited an oxygen isotopic shift as listed in Table 1. The 971.6 cm^{-1} band split into two bands at 935.7 and 935.0 cm^{-1} in $^{18}O_2$ spectrum, indicating that there are two components at 971.6 cm^{-1}. The 935.0 cm^{-1} band was destroyed on photolysis, while the 935.7 cm^{-1} band was not. An additional Cr + 1.0% D_2/0.5%O_2/Ar experiment was done, the spectra exhibited the same annealing and photolysis behavior with the Cr + H_2/O_2/Ar experiment, and the absorptions of species **2** and **3** shifted the same amount as in the CrO_3 + D_2/Ar experiments. The 971.6 cm^{-1} band in the Cr + H_2/O_2/Ar spectrum now split into two bands at 972.5 and 971.7 cm^{-1}; the former disappeared on photolysis while the latter did not.

A complementary experiment was done with a Cr target and 1.0% H_2 in argon. No product absorption was observed on

TABLE 2: Calculated Geometric Parameters (Bond Lengths in Ångstroms, Bond Angles in Degrees), Vibrational Frequencies (cm^{-1}), and Intensities (km/mol) for Chromium Oxides

molecule	geometry	frequency (intensity, mode)
CrO ($^5\Pi$)	1.616	867.5 (173)
CrO_2 ($^3B_1$)	1.598, 132.0	1032.2 (488, b_2), 988.8 (24, a_1), 224.9 (42, a_1)
CrO_2 ($^1A_1$)	1.589, 127.0	1032.8 (462, b_2), 1031.7 (20, a_1), 242.9 (51, a_1)
CrO_3 ($^1A_1$)	1.578, 115.4	1076.6 (480, e), 1003.1 (6, a_1), 375.5 (0, e), 202.4 (81, a_1)
(η^2-O_2)CrO_2 ($^3A_2$)	O−O:1.305, (O_2)−Cr:1.932, Cr−O:1.572, ∠OCrO:119.2	1216.6 (71, a_1), 1069.5 (323, b_2), 1061.0 (66, a_1), 547.8 (21, a_1), 521.3 (1, b_1), 316.6 (0, a_1), 237.6 (0, a_2), 189.4 (3, b_2), 160.0 (34, b_1)
H_2 ($^1\Sigma_g^+$)	0.744	4423.3 (0)

TABLE 3: Calculated Vibrational Frequencies (cm^{-1}) and Intensities (km/mol) for the Structures Described in Figure 5

molecule	frequency (intensity, mode)
(η^2-H_2)CrO_2 ($^3B_1$)	3950.0 (12, a_1), 1121.9 (25, b_1), 1037.3 (437, b_2), 1007.5 (23,a_1), 740.3 (25, a_1), 312.0 (0, a_2), 269.2 (19, a_1), 215.6 (5, b_2), 153.1 (5, b_1)
HCrO(OH) ($^3A''$)	3909.8 (243, a′), 1839.8 (143, a′), 1076.9 (214, a′), 760.7 (121, a′), 624.5 (19, a′), 480.7 (117, a′), 425.7 (190, a″), 207.5 (16, a′), 158.6 (14, a″)
$Cr(OH)_2$ ($^5A''$)	3898.8 (48, a′), 3896.5 (164, a″), 740.3 (251, a″), 624.3 (20, a′), 535.0 (134, a″), 465.9 (105, a′), 346.9 (48, a″), 300.8 (173, a′), 65.3 (0.5, a′)
(η^2-H_2)$_2CrO_2$ ($^1A_1$)	3129.0 (136, a_1), 3119.4 (168, b_2), 1668.1 (6, a_1), 1649.3 (20, b_2), 1105.8 (5, a_1), 1070.7 (319, b_1), 1020.0 (109, b_2), 993.0 (87, a_1), 862.9 (0, a_2), 783.2 (9, b_1), 645.6 (38, a_1), 425.6 (0, a_2), 418.1 (25, b_1), 321.6 (11, a_1), 247.0 (0.4,b_2)
(η^2-H_2)CrO_3	3938.1 (32, a′), 1279.0 (21, a′), 1068.5 (217, a″), 1060.7 (214, a′), 1000.7 (6, a′), 891.4 (1, a′), 373.2 (0, a′), 370.9 (1, a″), 338.3 (11, a″), 280.0 (25, a′), 266.5 (45, a′), 118.5 (2, a″)
TS	1948.1, 1794.1, 1079.2, 1069.4, 961.6, 880.3, 270.7, 145.4, 1293.3i

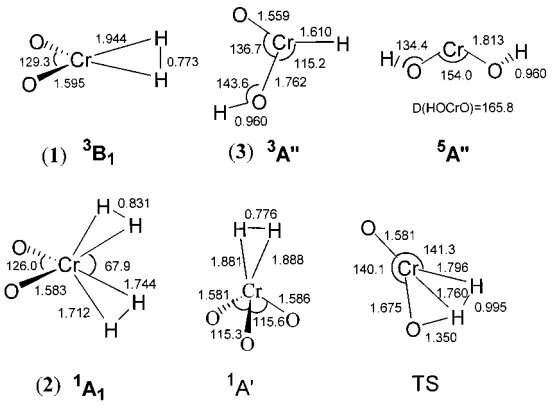

Figure 5. Optimized structures of (η^2-H_2)CrO_2, HCrO(OH), $Cr(OH)_2$, (η^2-H_2)$_2CrO_2$, and the transition state. Bond lengths are in ångstroms, and bond angles in degrees.

sample deposition, while very weak CrH_2 absorption at 1614.5 cm^{-1} was produced on broad-band photolysis.[14]

Calculation Results. We first calculated the states and geometries of pure chromium oxide as a test case. The calculated geometric parameters and vibrational frequencies are listed in Table 2. In agreement with high-level CCSD(t) calculations,[34] the ground state of CrO was predicted to be $^5\Pi$. The ground state of CrO_2 is a triplet ($^3B_1$). The calculated frequencies compare favorably to that observed in solid argon.[31,32] The lowest $^1A_1$ singlet state CrO_2 was predicted to be 24.0 kcal/mol higher in energy. The ground state of CrO_3 is $^1A_1$ with C_{3v} symmetry. The (η^2-O_2)CrO_2 molecule was calculated to have a $^3A_2$ ground state with C_{2v} symmetry.

We have optimized three H_2CrO_2 isomers, namely, (η^2-H_2)-CrO_2, HCrO(OH), and $Cr(OH)_2$. The optimized geometric parameters are shown in Figure 5, and the vibrational frequencies and intensities are listed in Table 3. The (η^2-H_2)CrO_2 molecule was predicted to have a triplet ground state ($^3B_1$) with pseudotetrahedral C_{2v} symmetry. The HCrO(OH) molecule was calculated to have a triplet ground state with a planar structure. For $Cr(OH)_2$, the lowest energy state is a quintet, corresponding to four unpaired electrons. At the B3LYP/6-311++G(d,p) level of theory, the $Cr(OH)_2$ molecule was calculated to be the most stable, followed by the HCrO(OH) and the (η^2-H_2)CrO_2 molecules, which were 22.3 and 47.9 kcal/mol higher in energy than the $Cr(OH)_2$, respectively.

Geometry optimization was also done for the (η^2-H_2)$_2CrO_2$ molecule on both singlet and triplet potential energy surfaces. The lowest state was calculated to be an $^1A_1$ state with C_{2v} symmetry, in which the two H_2 lie in the same plane that is perpendicular to the OCrO plane. Geometry optimization on the triplet energy surface without symmetry restriction converged to (η^2-H_2)CrO_2($^3B_1$) + H_2.

Similar calculations were also done on (η^2-H_2)CrO, and no stable structure was found. For the (η^2-H_2)CrO_3 molecule, geometry optimization found a $^1A'$ singlet ground state, as shown in Figure 5.

Assignments. *(η^2-H_2)CrO_2.* The 971.6 cm^{-1} band shifted to 972.5 cm^{-1} with D_2, and to 935.0 cm^{-1} with $^{18}O_2$. In experiments using the H_2 + D_2 mixture, a doublet feature was observed, showing that one H_2 moiety is involved in this mode. The oxygen isotopic ratio of 1.0391 indicates that this band is mainly due to an antisymmetric OCrO stretching vibration. The 6.3 cm^{-1} blue shift from the antisymmetric OCrO stretching vibration of CrO_2 (965.3 cm^{-1}) suggests that this band is due to the H_2−CrO_2 complex. Accordingly, we assign the 971.6 cm^{-1} band to the antisymmetric OCrO stretching vibration of the (η^2-H_2)CrO_2 molecule.

As shown in Figure 5, the (η^2-H_2)CrO_2 molecule was predicted to have a $^3B_1$ ground state with pseudotetrahedral C_{2v} symmetry, in which the HCrH plane is perpendicular to the OCrO plane. The H−H distance in (η^2-H_2)CrO_2 was calculated to be 0.773 Å, lengthened by about 0.029 Å compared with that in free H_2. The antisymmetric OCrO mode was calculated at 1037.3 cm^{-1} (437 km/mol), just 5.1 cm^{-1} higher than that of the CrO_2 calculated at the same level. The H−H, symmetric Cr−H, and OCrO stretching vibrational modes were predicted at 3950.0 (12 km/mol), 1121.9 (25 km/mol), and 1007.5 cm^{-1} (23 km/mol). These three modes are much less intense than that of the antisymmetric OCrO mode and were not observed in the present experiments.

$(\eta^2$-$H_2)_2CrO_2$. Absorptions at 2728.6 (0.04), 2640.5 (0.10), 1877.7 (0.02), 1724.1 (0.08), 999.2 (1.00), 903.8 (0.30), 890.3 (0.93), and 624.0 (0.15) cm^{-1} are assigned to different modes of the $(\eta^2$-$H_2)_2CrO_2$ molecule (values in parentheses are normalized relative intensities). These bands were observed in both $CrO_3 + H_2$ and $Cr + O_2/H_2$ experiments and maintained the same relative intensities throughout all the experiments, suggesting that they were due to different vibrational modes of the same molecule. The most intense band at 999.2 cm^{-1} and additional weak satellite features at 996.1 and 993.2 cm^{-1} showed natural abundance Cr isotopic intensity distributions (^{52}Cr, 83.8%, ^{53}Cr, 9.6%; ^{54}Cr, 2.4%), and clearly indicates one chromium atom involvement. The 999.2 cm^{-1} band shifted to 995.4 cm^{-1} with D_2 and to 963.8 cm^{-1} with $^{18}O_2$. The isotopic $^{52}Cr/^{53}Cr$ ratio of 1.0031 and $^{16}O/^{18}O$ ratio of 1.0367 are indicative of an antisymmetric OCrO stretching vibration. In the mixed $H_2 + D_2$ experiments, a triplet at 999.2, 997.8, and 995.4 cm^{-1} was observed, indicating that two equivalent H_2 molecules are involved in this molecule. The 903.8 and 890.3 cm^{-1} bands went to 707.6 and 675.6 cm^{-1} with D_2 and gave isotopic H/D ratios of 1.2773 and 1.3178. In the mixed $H_2 + D_2$ experiments, two intermediates at 897.3 and 690.0 cm^{-1} were observed, which also indicates that two equivalent H_2 molecules are involved in these two modes. The 897.3 and 690.0 cm^{-1} intermediate bands are due to Cr−H_2 and Cr-D_2 stretching vibrations of the $(\eta^2$-$H_2)(\eta^2$-$D_2)CrO_2$ molecule. In the $H_2 + HD + D_2$ experiment, extra intermediates at 899.9, 899.1, 780.8, 772.5, 767.3, 764.3, 751.6, 687.7, and 686.8 cm^{-1} were observed. This isotopic structure indicates that the H atoms in each H_2 are inequivalent. The 899.9 and 899.1 cm^{-1} bands are due to Cr−H_2 stretching vibrations of the $(\eta^2$-$H_2)(\eta^2$-x$)CrO_2$ (x = HD or DH) molecules, the 687.7 and 686.8 cm^{-1} bands are Cr-D_2 stretching vibrations of the $(\eta^2$-$D_2)(\eta^2$-x$)CrO_2$ (x = HD or DH) molecules, and the intermediates between 780.8 and 751.6 cm^{-1} are due to Cr−(HD) stretching vibrations of the $(\eta^2$-HD$)(\eta^2$-x$)CrO_2$ (x = H_2, HD, or D_2) molecules. The 2728.6 and 2640.5 cm^{-1} bands are symmetric and antisymmetric H−H stretching vibrations, but the mixed isotopic structures could not be observed due to isotopic dilutions. The 1724.1 and 1332.4 cm^{-1} bands are assigned to the combination bands of symmetric and antisymmetric Cr−H_2 and Cr−D_2 stretching modes for $(\eta^2$-$H_2)_2CrO_2$ and $(\eta^2$-$D_2)_2CrO_2$. These two bands fall 70.0 and 50.8 cm^{-1} below the sum of the a_1 and b_2 Cr−H_2 (or D_2) stretching fundamentals. The 1877.7 cm^{-1} band is assigned to the combination band of symmetric and antisymmetric OCrO stretching modes for $(\eta^2$-$H_2)_2CrO_2$. The 624.0 cm^{-1} band shifted to 457.1 cm^{-1} with D_2 and gave a H/D ratio of 1.3651. This band is assigned to the H_2−Cr−H_2 bending vibration for $(\eta^2$-$H_2)_2CrO_2$.

The identification of $(\eta^2$-$H_2)_2CrO_2$ is supported by DFT calculations. The $(\eta^2$-$H_2)_2CrO_2$ molecule was predicted to have an $^1A_1$ ground state with a C_{2v} symmetry in which the two H_2 fragments lie in the same plane that is perpendicular to the OCrO plane. The two H_2 subunits are equivalent, but the H atoms in each H_2 are slightly inequivalent. A comparison of the experimentally observed and calculated IR absorptions and isotopic frequency ratios is listed in Table 4. The harmonic frequencies calculated for $(\eta^2$-$H_2)_2CrO_2$ deviate from the experimental values by the amounts expected when anharmonicity of the vibrations is not taken into considerations.[35,36]

HCrO(OH). Absorptions at 1012.3, 1753.1, and 3714.2 cm^{-1} appeared only on broad-band photolysis when the $(\eta^2$-$H_2)CrO_2$ and $(\eta^2$-$H_2)_2CrO_2$ absorptions greatly decreased. These three bands exhibited 0.45:0.30:1.00 normalized relative intensities.

TABLE 4: Comparison between Experimental Observed and DFT Calculated Vibrational Frequencies (cm^{-1}) and Isotopic Frequency Ratios for $(\eta^2$-$H_2)CrO_2$ (1), $(\eta^2$-$H_2)_2CrO_2$ (2) and HCrO(OH) (3)

	mode	experimental			calculation		
species	mode	freq	H/D	$^{16}O/^{18}O$	freq	H/D	$^{16}O/^{18}O$
1	H−H				3950.0	1.4136	1.0000
	Cr−H_2				1121.9	1.4116	1.0000
	asym OCrO	971.6	0.9991	1.0391	1037.3	1.0000	1.0393
	sym OCrO				1007.5	1.0031	1.0498
2	sym H−H	2728.6	1.3579		3129.0	1.4130	1.0000
	asym H−H	2640.5	1.3410		3119.4	1.4126	1.0000
	sym OCrO		1.0658		1105.8	1.0480	1.0162
	asym OCrO	999.2	1.0038	1.0367	1070.7	1.0058	1.0372
	asym H_2CrH_2	890.3	1.3178	1.0000	1020.0	1.3840	1.0000
	sym H_2CrH_2	903.8	1.2773	1.0309	993.0	1.3261	1.0349
	H_2CrH_2 bend.	624.0	1.3651	1.0008	645.6	1.3881	1.0006
3	O−H str	3714.2	1.3551	1.0031	3909.8	1.3723	1.0034
	Cr−H str	1753.1	1.3831	1.0000	1839.8	1.3987	1.0000
	Cr−O str	1012.3	1.0005	1.0419	1076.9	1.0010	1.0433

The 1012.3 cm^{-1} band showed a very small (0.5 cm^{-1}) deuterium shift but a large oxygen-18 shift (40.7 cm^{-1}). The $^{16}O/^{18}O$ isotopic ratio of 1.0419 indicates that this band is mainly due to a terminal Cr−O stretching vibration. The 1753.1 cm^{-1} band exhibited no oxygen-18 isotopic shift and was shifted to 1267.5 cm^{-1} with D_2. The H/D isotopic ratio 1.3831 is characteristic of a Cr−H stretching mode.[14] The 3714.2 cm^{-1} band gave a deuterium counterpart at 2740.9 cm^{-1}, which defines a H/D isotopic ratio of 1.3551. The oxygen-18 counterpart was observed at 3702.7 cm^{-1} and gave a $^{16}O/^{18}O$ ratio of 1.0031. The deuterium and oxygen isotopic shifts suggest that this band originated from an O−H stretching vibration. In both the mixed $H_2 + D_2$ and $H_2 + HD + D_2$ experiments, no intermediate absorption was observed for the 1753.1 and 3714.2 cm^{-1} bands, indicating that only one H atom is involved in each mode. Accordingly, the 1012.3, 1753.1, and 3714.2 cm^{-1} bands are assigned to the Cr−O, Cr−H, and O−H stretching vibrations of the HCrO(OH) molecule.

The HCrO(OH) molecule was calculated to have an $^3A''$ ground state with planar geometry. As listed in Table 4, the calculated frequencies and isotopic frequency ratios provide good support for the proposed identification of this molecule.

Although CrO_3 and CrO molecules were also produced on laser ablation of CrO_3, no reaction product from CrO or CrO_3 with H_2 was found. As has been mentioned, DFT calculations predicted that CrO does not form a stable complex with H_2. CrO_3 was predicted to form a stable $(\eta^2$-$H_2)CrO_3$ complex with two strong OCrO stretching vibrations at 1060.7 and 1068.5 cm^{-1}, red shifted about 8.1 and 15.9 cm^{-1} from the CrO_3 absorption predicted at 1076.6 cm^{-1}.

Bonding Considerations. The bonding of transition metal dihydrogen complexes involve electron donation from the H_2 σ bonding orbital to the metal and metal electron back-donation to the H_2 σ^* antibonding orbital.[5,6] The $^3B_1$ ground state $(\eta^2$-$H_2)CrO_2$ has an electron configuration of $(core)(b_1)^1(a_1)^1(a_1)^0$. The molecule can be viewed as the interaction of a $^3B_1$ CrO_2 fragment and a H_2 fragment. As shown in Scheme 1, the LUMO a_1 orbital of CrO_2 is primarily a hybrid of the Cr 4s and $3d_{z^2}$ orbitals that are polarized away from the O atoms. This orbital is the primary acceptor orbital for σ donation from the side-bonded H_2 fragment. It can interact with the σ molecular orbital of H_2 regardless of the rotational orientation of the H_2. The filled b_1 orbital is the CrO_2 π MO and is the principal back-donation orbital. It interacts with the σ^* antibonding MO of H_2 in $(\eta^2$-$H_2)CrO_2$, which favors the pseudotetrahedral C_{2v} symmetry over the planar C_{2v} symmetry for $(\eta^2$-$H_2)CrO_2$. Population analysis

SCHEME 1: Principal Orbital Interaction in (η^2-H_2)CrO_2

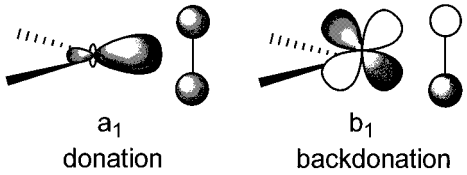

SCHEME 2: Principal Orbital Interaction in (η^2-H_2)$_2CrO_2$

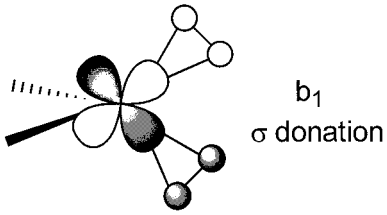

indicated that H_2 transfers about 0.1 e to the CrO_2 subunit, while CrO_2 back-donates about 0.03 e to H_2.

The ground state of (η^2-H_2)$_2CrO_2$ is an $^1A_1$ state that correlates to CrO_2 ($^1A_1$) + $2H_2$ with an electron configuration of (core)-$(a_1)^2(b_1)^0(a_1)^0$. Since the b_1 LUMO of $^1A_1$ CrO_2 involves Cr $3d_{xz}$ and O $2p_x$ orbitals and is the Cr−O bonding orbital, σ donation is strongly favored. This b_1 orbital is oriented in the plane perpendicular to the plane of the CrO_2 subunit. As shown in Scheme 2, the b_1 orbital can interact with the σ molecular orbitals of the two H_2 in the plane perpendicular to the CrO_2 plane. The a_1 doubly occupied HOMO corresponds to the nonbonding orbitals of a singlet CrO_2 and is the principal back-donation orbital. The back-donation of Cr 3d electrons to the σ^* antibonding orbitals of H_2 stabilized the HOMO a_1 orbital, which favors a closed-shell electronic structure. NBO population analysis showed that each H_2 subunits transfers about 0.25 e to the CrO_2 moiety, while there is about 0.1 e back-donation from CrO_2 to each H_2 subunit. The large back-donation is responsible for the lengthening of the H−H bonds (0.831 Å) in (η^2-H_2)$_2$-CrO_2 compared to the 0.773 Å in (η^2-H_2)CrO_2. This is a typical result of the difference between one-electron back-donation and two-electron back-donation.[37]

The binding energy of $^3B_1$ (η^2-H_2)CrO_2 with respect to CrO_2-($^3B_1$) + H_2($^1\Sigma_g^+$) was calculated to be 8.6 kcal/mol, after zero point energy correction. Due to large σ donation and π back-donation, (η^2-H_2)$_2CrO_2$ is more strongly bound than (η^2-H_2)-CrO_2. The binding energy per H_2 in (η^2-H_2)$_2CrO_2$ was estimated to be 18.0 kcal/mol with respect to the CrO_2($^1A_1$) + $2H_2$($^1\Sigma_g^+$) asymptote. Accordingly, the calculated binding energy of singlet state (η^2-H_2)CrO_2 ($^1A_1$) is 18.9 kcal/mol, correlating to CrO_2-($^1A_1$) + H_2($^1\Sigma_g^+$).

Reaction Mechanism. Laser ablation of a CrO_3 target produces CrO_2 as the major product. The (η^2-H_2)CrO_2 and (η^2-H_2)$_2CrO_2$ molecules are formed by reactions between CrO_2 and H_2 molecules, reactions 1 and 2, which were calculated to be exothermic:

$$CrO_2(^3B_1) + H_2(^1\textstyle\sum_g^+) \rightarrow (\eta^2\text{-}H_2)CrO_2(^3B_1) \qquad \Delta E = -8.6 \text{ kcal/mol} \quad (1)$$

$$(\eta^2\text{-}H_2)CrO_2 + H_2(^1\textstyle\sum_g^+) \rightarrow (\eta^2\text{-}H_2)_2CrO_2(^1A_1) \qquad \Delta E = -3.4 \text{ kcal/mol} \quad (2)$$

The absorptions of (η^2-H_2)CrO_2 and (η^2-H_2)$_2CrO_2$ increased on annealing in low H_2 concentration experiments, suggesting that reactions 1 and 2 require negligible activation energy.

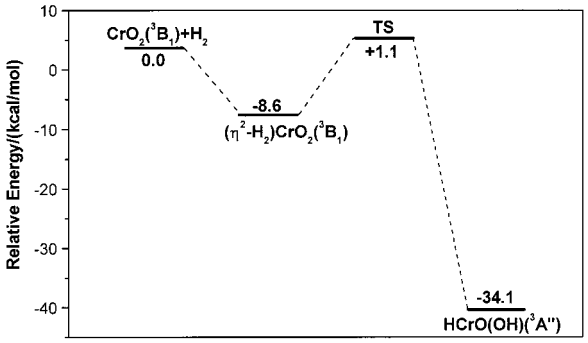

Figure 6. Potential energy surface following the $CrO_2 + H_2 \rightarrow$ HCrO-(OH) reaction path. Energies given are in kcal/mol and are relative to the separated ground-state reactants: CrO_2 ($^3B_1$) + H_2.

The HCrO(OH) molecule was only produced upon photolysis when the (η^2-H_2)CrO_2 absorption was destroyed, this suggests that the HCrO(OH) molecules were generated from (η^2-H_2)-CrO_2 via reaction 3. The (η^2-H_2)$_2CrO_2$ absorptions also decreased on photolysis. The (η^2-H_2)$_2CrO_2$ molecule may lose one H_2 to form (η^2-H_2)CrO_2, which can be rearranged to HCrO-(OH).

$$(\eta^2\text{-}H_2)CrO_2(^3B_1) \rightarrow HCrO(OH)(^3A'') \qquad \Delta E = -25.5 \text{ kcal/mol} \quad (3)$$

Figure 6 shows the potential energy surface from CrO_2 + H_2 leading to HCrO(OH). From (η^2-H_2)CrO_2, one H atom transfers from Cr to one oxygen to form HCrO(OH). This H transfer occurs via a four-center transition state like in a σ bond metathesis and such transition states have been shown to be low in energy by several theoretical works on gas-phase chemistry.[38] The calculated structural parameters of this transition state are given in Figure 5. The energy barrier was predicted to be 9.7 kcal/mol.

From HCrO(OH), the second H atom could also transfer from Cr to O to form $Cr(OH)_2$ via reaction 4, which was predicted to be exothermic. This reaction should have a high energy barrier

$$HCrO(OH)(^3A'') \rightarrow Cr(OH)_2(^5A'') \; \Delta E = -22.4 \text{ kcal/mol} \quad (4)$$

and was not observed with our experimental conditions. Although one could imagine formation of $Cr(OH)_2$ from (η^2-H_2)$_2CrO_2$, it seems that (η^2-H_2)$_2CrO_2$ prefers to lose a H_2 ligand on broad-band photolysis.

In the Cr + H_2/O_2/Ar experiments, sample deposition at 11 K produced the CrO_2 and (η^2-O_2)CrO_2 absorptions, with no (η^2-H_2)CrO_2 and (η^2-H_2)$_2CrO_2$ absorptions. This may imply that CrO_2 is more easily ligated with O_2 than H_2 during the co-condensation process. The binding energy of (η^2-O_2)CrO_2 with respect to CrO_2($^3B_1$) + O_2($^3\Sigma_g^-$) was predicted to be 40.3 kcal/mol, significantly higher than the binding energy of (η^2-H_2)-CrO_2 (8.6 kcal/mol). During the co-condensation process, H_2 can be easily replaced by O_2. For comparison, we note that the CrO_3 + H_2/Ar experiments employed lower laser power than the Cr + H_2/O_2/Ar experiments, but the (η^2-H_2)CrO_2 and (η^2-H_2)$_2CrO_2$ absorptions were observed on sample deposition even with lower H_2 concentrations (0.4%). Apparently, low laser power ablation of the CrO_3 target produced negligible O_2 molecules, and almost no (η^2-O_2)CrO_2 absorption was observed.

On lower temperature (18 K) sample annealing, H_2 molecules are mobile in solid argon. They can diffuse and then react with

CrO_2 to form the $(\eta^2\text{-}H_2)CrO_2$ and $(\eta^2\text{-}H_2)_2CrO_2$ molecules. The O_2 molecules are much more difficult to diffuse in solid argon than H_2 molecules at such a low temperature as 18 K.

Conclusions

The first chromium dioxide dihydrogen and bis-dihydrogen complexes, $(\eta^2\text{-}H_2)CrO_2$ and $(\eta^2\text{-}H_2)_2CrO_2$, have been prepared by co-condensation of the CrO_2 molecules generated from laser ablation of CrO_3 with H_2 in excess argon at 11 K. Broad-band photolysis of the $(\eta^2\text{-}H_2)CrO_2$ complex produced the HCrO(OH) molecule. Laser-ablated Cr atoms reacted with H_2/O_2 mixtures to give primarily the CrO_2 and $(\eta^2\text{-}O_2)CrO_2$ molecules, while the $(\eta^2\text{-}H_2)CrO_2$, $(\eta^2\text{-}H_2)_2CrO_2$, and HCrO(OH) molecules were also produced on annealing and photolysis.

Density functional theoretical calculations using the B3LYP functional have been employed to support assignments of the aforementioned species. The $(\eta^2\text{-}H_2)CrO_2$ molecule was predicted to have a $^3B_1$ ground state with pseudotetrahedral C_{2v} symmetry. The binding energy with respect to CrO_2 ($^3B_1$) + H_2 was computationally estimated to be 8.6 kcal/mol. The $(\eta^2\text{-}H_2)_2CrO_2$ complex has a $^1A_1$ ground state and is more strongly bound than the $(\eta^2\text{-}H_2)CrO_2$ complex due to large σ donation and π back-donation. The binding energy per H_2 in $(\eta^2\text{-}H_2)_2\text{-}CrO_2$ was estimated to be 18.0 kcal/mol. In addition, the potential energy surface along the $CrO_2 + H_2 \rightarrow$ HCrOH reaction path has also been calculated.

Acknowledgment. We gratefully acknowledge support from NSFC (Grant No. 20003003) and the Chinese NKBRSF.

References and Notes

(1) See for example: Esteruelas, M. A.; Ore, L. A. *Chem. Rev.* **1998**, *98*, 577.

(2) Kubas, G. J.; Ryan, R. B.; Swanson, B. L.; Vergamini, P. J.; Wasserman, H. J. *J. Am. Chem. Soc.* **1984**, *106*, 451.

(3) Maseras, F.; Lledos, A. *Chem. Rev.* **2000**, *100*, 601.

(4) Heinekey, D. M.; Oldham, W. J. *Chem. Rev.* **1993**, *93*, 913.

(5) Kemper, P. R.; Weis, P.; Bowers, M. T.; Maitre, P. *J. Am. Chem. Soc.* **1998**, *120*, 13494.

(6) Maitre, P.; Bauschlicher, C. W., Jr. *J. Phys. Chem.* **1993**, *97*, 11912.

(7) Sweany, R. L. *J. Am. Chem. Soc.* **1985**, *107*, 2374.

(8) Upmacis, R. K.; Gadd, G. E.; Poliakoff, M.; Simpson, M. B.; Turner, J. J.; Whyman, R.; Simpson, A. F. *J. Chem. Soc., Chem. Commun*. **1985**, 27.

(9) Jackson, S. A.; Hodges, P. M.; Poliakoff, M.; Turner, J. J.; Grevels, F. W. *J. Am. Chem. Soc.* **1990**, *112*, 1221. Howdle, S. M.; Healy, M. A.; Poliakoff, M. *J. Am. Chem. Soc.* **1990**, *112*, 4804.

(10) Dapprich, S.; Frenking, G. *Angew. Chem., Int. Ed. Engl.* **1995**, *34*, 354.

(11) Pacchioni, G. *J. Am. Chem. Soc.* **1990**, *112*, 80.

(12) Jean, Y.; Eisenstein, O.; Volatron, F.; Maouche, B.; Sefta, F. *J. Am. Chem. Soc.* **1986**, *108*, 6587.

(13) Zee, R. J.; DeVore, T. C.; Weltner, W., Jr. *J. Chem. Phys*. **1979**, *71*, 2051.

(14) Xiao, Z. L.; Hauge, R. H.; Margrave, J. L. *J. Phys. Chem.* **1992**, *96*, 636.

(15) Ma, B.; Collins, C. L.; Schaefer, H. F. *J. Am. Chem. Soc.* **1996**, *118*, 870.

(16) Martinez, A. *J. Phys. Chem. A* **1998**, *102*, 1381.

(17) Cook, G. K.; Mayer, J. M. *J. Am. Chem. Soc*. **1994**, *116*, 1855.

(18) Fiedler, A.; Kretzschmar, H.; Schroder, D.; Schwarz, H. *J. Am. Chem. Soc.* **1996**, *118*, 9941.

(19) Kang, H.; Beauchamp, J. L. *J. Am. Chem. Soc.* **1986**, *108*, 5663.

(20) Chen, M. H.; Wang, X. F.; Zhang, L. N.; Yu, M.; Qin, Q. Z. *Chem. Phys.* **1999**, *242*, 81. Zhou, M. F.; Zhang, L. N.; Qin, Q. Z. *J. Am. Chem. Soc.* **2000**, *122*, 4483.

(21) Bauschlicher, C. W., Jr.; Ricca, A.; Partridge, H.; Langhoff, S. R. In *Recent Advances in Density Functional Theory*; Chong, D. P., Ed.; World Scientific Publishing: Singapore, 1997: Part II.

(22) Siegbahn, P. E. M. In *Electronic Structure Calculations for Molecules Containing Transition Metals.* Advances in Chemistry and Physics XCIII; Wiley: New York, 1996.

(23) Zhou, M. F.; Zhang, L. N.; Chen, M. H.; Zheng, Q. K.; Qin, Q. Z. *J. Phys. Chem. A* **2000**, *104*, 10159. Zhou, M. F.; Zhang, L. N.; Dong, J.; Qin, Q. Z. *J. Am. Chem. Soc*. **2000**, *122*, 10680.

(24) Frisch, M. J.; Trucks, G. W.; Schlegel, H. B.; Scuseria, G. E.; Robb, M. A.; Cheeseman, J. R.; Zakrzewski, V. G.; Montgomery, J. A., Jr.; Stratmann, R. E.; Burant, J. C.; Dapprich, S.; Millam, J. M.; Daniels, A. D.; Kudin, K. N.; Strain, M. C.; Farkas, O.; Tomasi, J.; Barone, V.; Cossi, M.; Cammi, R.; Mennucci, B.; Pomelli, C.; Adamo, C.; Clifford, S.; Ochterski, J.; Petersson, G. A.; Ayala, P. Y.; Cui, Q.; Morokuma, K.; Malick, D. K.; Rabuck, A. D.; Raghavachari, K.; Foresman, J. B.; Cioslowski, J.; Ortiz, J. V.; Baboul, A. G.; Stefanov, B. B.; Liu, G.; Liashenko, A.; Piskorz, P.; Komaromi, I.; Gomperts, R.; Martin, R. L.; Fox, D. J.; Keith, T.; Al-Laham, M. A.; Peng, C. Y.; Nanayakkara, A.; Gonzalez, C.; Challacombe, M.; Gill, P. M. W.; Johnson, B.; Chen, W.; Wong, M. W.; Andres, J. L.; Gonzalez, C.; Head-Gordon, M.; Replogle, E. S.; Pople, J. A. *Gaussian 98*, revision A.7; Gaussian, Inc.: Pittsburgh, PA, 1998.

(25) Becke, A. D. *J. Chem. Phys*. **1993**, *98*, 5648.

(26) Lee, C.; Yang, E.; Parr, R. G. *Phys. Rev. B* **1988**, *37*, 785.

(27) McLean, A. D.; Chandler, G. S. *J. Chem. Phys*. **1980**, *72*, 5639. Krishnan, R.; Binkley, J. S.; Seeger, R.; Pople, J. A. *J. Chem. Phys*. **1980**, *72*, 650.

(28) Wachter, J. H. *J. Chem. Phys.* **1970**, *52*, 1033. Hay, P. J. *J. Chem. Phys*. **1977**, *66*, 4377.

(29) Head-Gordon, M.; Pople, J. A.; Frisch, M. *Chem. Phys. Lett*. **1988**, *153*, 503.

(30) Reed, A. E.; Curtiss, L. A.; Weinhold, F. *Chem. Rev.* **1988**, *88*, 899.

(31) Almond, M. J.; Hahne, M. *J. Chem. Soc., Dalton Trans.* **1988**, 2255.

(32) Chertihin, G. V.; Bare, W. D.; Andrews, L. *J. Chem. Phys.* **1997**, *107*, 2798; Zhou, M. F.; Andrews, L. *J. Chem. Phys.* **1999**, *111*, 4230.

(33) Chertihin, G. V.; Andrews, L. *J. Chem. Phys*. **1998**, *108*, 6404; Zhou, M. F.; Hacaloglu, J.; Andrews, L. *J. Chem. Phys*. **1999**, *110*, 9450.

(34) Bauschlicher, C. W., Jr.; Maitre, P. *Theor. Chim. Acta* **1995**, *90*, 189.

(35) Plitt, H. S.; Bar, M. R.; Ahlrichs, R.; Schnockel, H. *Angew. Chem., Int. Ed. Engl.* **1991**, *30*, 832.

(36) Andrews, L.; Manceron, L.; Alikhani, M. E.; Wang, X. F. *J. Am. Chem. Soc.* **2000**, *122*, 11011.

(37) Maitre, P.; Bauschlicher, C. W., Jr. *J. Phys. Chem.* **1995**, *99*, 6836.

(38) See for example: Weisshaar, J. C. *Acc. Chem. Res*. **1993**, *26*, 213. Carroll, J. J.; Haug, K. L.; Weisshaar, J. C.; Blomberg, M. R. A.; Siegbahn, P. E. M.; Svensson, M. *J. Phys. Chem.* **1995**, *99*, 13955.